

Koopman neural operator as a mesh-free solver of non-linear partial differential equations*

Wei Xiong,[†] Xiaomeng Huang,[†] Ziyang Zhang,[‡] Ruixuan Deng,[§] Pei Sun,[¶] and Yang Tian^{**}

The lacking of analytic solutions of diverse partial differential equations (PDEs) gives birth to series of computational techniques for numerical solutions. In machine learning, numerous latest advances of solver designs are accomplished in developing neural operators, a kind of mesh-free approximators of the infinite-dimensional operators that map between different parameterization spaces of equation solutions. Although neural operators exhibit generalization capacities for learning an entire PDE family simultaneously, they become less accurate and explainable while learning long-term behaviours of non-linear PDE families. In this paper, we propose Koopman neural operator (KNO), a new neural operator, to overcome these challenges. With the same objective of learning an infinite-dimensional mapping between Banach spaces that serves as the solution operator of target PDE family, our approach differs from existing models by formulating a non-linear dynamic system of equation solution. By approximating the Koopman operator, an infinite-dimensional linear operator governing all possible observations of the dynamic system, to act on the flow mapping of dynamic system, we can equivalently learn the solution of an entire non-linear PDE family by solving simple linear prediction problems. In zero-shot prediction and long-term prediction experiments on representative PDEs (e.g., the Navier-Stokes equation), KNO exhibits notable advantages in breaking the tradeoff between accuracy and efficiency (e.g., model size) while previous state-of-the-art models are limited. These results suggest that more efficient PDE solvers can be developed by the joint efforts from physics and machine learning.

In science and engineering, partial differential equation (PDE) is a fundamental tool to characterize various problems [1]. However, numerous important PDEs, such as the Navier-Stokes equation, still lack analytic solutions [2, 3]. Consequently, the urgent needs of solving complicated PDEs have given birth to diverse techniques for computationally approximating PDE solutions [4].

Given $\Phi = \Phi(D; \mathbb{R}^{d_\phi})$, a Banach space of inputs, and $\Gamma = \Gamma(D; \mathbb{R}^{d_\gamma})$, a Banach space of solutions, defined on a bounded open set $D \subset \mathbb{R}^d$, these PDE solvers are expected to approximate a solution operator \mathcal{O} that relates Φ with Γ for a typically time-dependent PDE family

$$\partial_t \gamma(x_t) = (\mathcal{L}_\phi \gamma)(x_t) + \eta(x_t), \quad x_t \in D \times T, \quad (1)$$

$$\gamma(x_t) = \gamma_B, \quad x_t \in \partial D \times T, \quad (2)$$

$$\gamma(x_0) = \gamma_I, \quad x_0 \in D \times \{0\}. \quad (3)$$

In Eq. (1-3), notions γ_B and γ_I denote the boundary and initial conditions, set $T = [0, \infty)$ is the time domain, differential operator \mathcal{L}_ϕ is characterized depending on ϕ , fixed function $\eta(\cdot)$ lives in a function space determined by \mathcal{L}_ϕ , and $\gamma(\cdot)$ is the solution of the PDE family. This formulation gives rise to the solution operator $\mathcal{O} : (\phi, \gamma_B, \gamma_I) \mapsto \gamma$. For convenience, we always consider fixed boundary and initial conditions in our derivations. In application, researchers always consider a parametric counterpart $\mathcal{O}_\theta \simeq \mathcal{O}$ parameterized by θ [5].

To date, diverse types of PDE solvers have been developed. In Sec. I of our supplementary materials (SM), we present a review of classic numerical and neural-network-based solvers. Compared with classic numerical solvers, neural-network-based solvers, especially neural operators, are more efficient in dealing with science and engineering questions where PDEs are increasingly com-

plicated [5, 6]. Therefore, our research primarily focus on neural operator, a kind of mesh-free PDE solver [5, 6].

Challenges. Despite the progress in theoretical foundations [7], approximator designs [6, 8], and applications [9], there still remain numerous challenges in existing neural operators, among which, a critical one lies in the limited capacity of existing models to learn the long-term dynamics of complicated PDEs.

Let us rethink about the iterative update strategy of neural operators for solving Eqs. (1)-(3) [5]. As suggested in Sec. II of supplementary materials (SM), the iteration is similar to a dynamic system perspective where we study the evolution mapping $\zeta : \mathbb{R}^{d_\gamma} \times T \rightarrow \mathbb{R}^{d_\gamma}$ of an infinite-dimensional non-linear dynamic system $\gamma_t = \gamma(D \times \{t\})$ (notion $\gamma(D \times \{t\})$ represents that function γ acts on all elements in $D \times \{t\}$)

$$\gamma_{t+\varepsilon} = \gamma_t + \int_t^{t+\varepsilon} \zeta(\gamma_\tau, \tau) d\tau, \quad \forall t \in T. \quad (4)$$

For non-linear PDE families, the evolution mapping ζ is even more intricate than the equation solution γ itself. The infinite-dimensional non-linear flow mapping ζ makes the accurate prediction of long-term dynamics of γ_t nearly impossible. To maintain accuracy, existing models are required to enlarge model size or complexity, inevitably facing the trade-off between accuracy and efficiency. Therefore, overcoming the limitation in learning long-term PDE behaviours is necessary for optimizing PDE solvers, which is the core objective of our research.

Our contribution. In this paper, we attempt to overcome the challenge of predicting long-term PDE dynamics by proposing a new neural operator named as Koopman neural operator (KNO). Besides learning the solu-

tion operator of an entire target PDE family, we formalize a non-linear dynamic system of equation solution described by Eq. (4) in the meanwhile. This characterization supports to optimize the iterative update strategy of neural operators using dynamic system theory. To capture intricate long-term dynamics, our model is designed to learn the Koopman operator, an infinite-dimensional linear operator governing all observations of a dynamic system, to act on the evolution mapping ζ of the dynamic system of equation solution. By doing so, we can transform the original task into an equivalent but simpler linear prediction problem. We compare KNO with existing state-of-the-art models (e.g. the Fourier neural operator [6]) in zero-shot and long-term prediction experiments with representative PDEs. While previous methods suffer from the tradeoff between accuracy and efficiency (e.g., model size), KNO is shown to achieve higher accuracy with a smaller model size.

Computational framework. We begin with formalizing the non-linear dynamic system of equation solution

$$\partial_t \gamma_t = \zeta(\gamma_t, t), \quad \forall \gamma_t \in \mathbb{R}^{d_\gamma} \times T, \quad (5)$$

which can be either non-autonomous (i.e., the flow mapping θ associated with $\zeta(\cdot, \cdot)$ is time-dependent) or autonomous (i.e., the flow mapping θ is time-independent such that $\partial_t \zeta(\cdot, t) \equiv 0$) in different PDE families. The cocycle property of the flow mapping θ [10]

$$\theta_t^{t'} = \theta_{t+\tau}^{t'} \circ \theta_t^{t+\tau}, \quad \forall t \leq t + \tau \leq t' \in T \quad (6)$$

defines how γ , the equation solution, evolves across adjoining time intervals, where notion \circ denotes the composition of mappings. The non-linear, and potentially non-autonomous, dynamic system in Eqs. (5-6) makes the long-term prediction of γ_t a daunting challenge.

Our idea originates from dynamic system theory. Given with an appropriate space defined by a set of observation function $\mathcal{G}(\mathbb{R}^{d_\gamma} \times T) = \{\mathbf{g} | \mathbf{g} : \mathbb{R}^{d_\gamma} \times T \rightarrow \mathbb{C}\}$, we may search a family of Koopman operators $\mathcal{K}_t^{t+\varepsilon} : \mathcal{G}(\mathbb{R}^{d_\gamma} \times T) \rightarrow \mathcal{G}(\mathbb{R}^{d_\gamma} \times T)$ parameterized by time difference ε to linearize the non-linear dynamics of γ_t [10]

$$\mathcal{K}_t^{t+\varepsilon} \mathbf{g}(\gamma_t) = \mathbf{g}(\theta_t^{t+\varepsilon}(\gamma_t)) = \mathbf{g}(\gamma_{t+\varepsilon}), \quad \forall t \leq t + \varepsilon \in T. \quad (7)$$

Therefore, after proposing an optimal approximation of \mathbf{g} , we can derive a linear evolution of γ_t in a new space

$$\partial_t \mathbf{g}(\gamma_t) = \lim_{\varepsilon \rightarrow 0} \frac{\mathcal{K}_t^{t+\varepsilon} \mathbf{g}(\gamma_t) - \mathbf{g}(\gamma_t)}{\varepsilon}, \quad (8)$$

which is beneficial to solving Eq. (5). Eq. (7) is generally applicable to both non-autonomous and autonomous dynamic systems. An autonomous case of Eq. (7) is presented in Sec. II in our supplementary materials (SM).

In mathematics, the adjoint of the Koopman operator defined by Eq. (8) is the Perron-Frobenius operator of

dynamic systems [11] while the adjoint of the associated Lie operator (see Sec. II in our supplementary materials (SM)) is the Liouville operator of Hamiltonian dynamics [12, 13]. These properties relate our idea with well-known theories about linear representation of dynamic systems in statistical physics and quantum mechanics [14].

The challenges underlying Eq. (7) arise from the non-triviality of approximating observation function \mathbf{g} and estimating the Koopman operator $\mathcal{K}_t^{t+\varepsilon}$. Different from existing machine-learning-based Koopman operator models that either are limited to autonomous dynamic systems (e.g., the case described by Eq. (7)) [15–18] or require *a priori* knowledge about the eigenvalue spectrum (e.g, the numbers of real and complex eigenvalues) of Koopman operator [19], we pursue to develop an approximation applicable to both non-autonomous and autonomous dynamic systems without strong requirement of *a priori* knowledge [20]. In Sec. III of supplementary materials (SM), we propose a computational framework to learn \mathbf{g} and $\mathcal{K}_t^{t+\varepsilon}$ based on the Krylov subspace method [21] and the Galerkin projection. This framework is valid as long as the target Koopman operator has a discrete spectrum [10] to support an invariant sub-space approximation. Because the on-line learning of a time-dependent operator $\mathcal{K}_t^{t+\varepsilon}$ may unavailable in application due to its high requirement on data size and computation resource, we further suggest $\bar{\mathcal{K}}_\varepsilon$, an expectation of the Koopman operator controlled by time resolution ε . This constant operator only requires economic off-line training and serves as a reasonable counterpart of $\mathcal{K}_t^{t+\varepsilon}$ under ergodic condition [22, 23]. Operator $\bar{\mathcal{K}}_\varepsilon$ is used as a default setting in our framework, yet one can freely modify it to a time-dependent operator if on-line training is accessible.

Neural network. Our neural network model, named as Koopman neural operator (KNO), not only implements the mathematics defined above but also utilizes various numerical techniques to optimize its efficiency. Below, we summarize the main architecture of KNO.

- (1) *Part 1: Observation.* An input $\phi_t = \phi(D \times \{t\})$ of the PDE is transformed into $\mathbf{g}(\hat{\gamma}_t)$ by an observation function $\mathbf{g}(\cdot)$ parameterized by an encoder.
- (2) *Part 2: Fourier transform.* To accelerate the iterative update strategy [6] and to extract the low-frequency information (i.e., main component and background) of the represented equation solution $\mathbf{g}(\hat{\gamma}_t)$, we apply the Fourier transform to map $\mathbf{g}(\hat{\gamma}_t)$ as $\mathbf{g}_F(\hat{\gamma}_t) = \mathcal{F} \circ \mathbf{g}(\hat{\gamma}_t)$ and truncate the Fourier series at ω , a maximum number of frequency modes. Compared with the truncated high-frequency information (i.e., perturbations), the remaining low-frequency information with more clear evolution patterns may be easier to learn.
- (3) *Part 3: Koopman operator approximator.* Given low-frequency information $\mathbf{g}_F(\hat{\gamma}_t)$, we define a

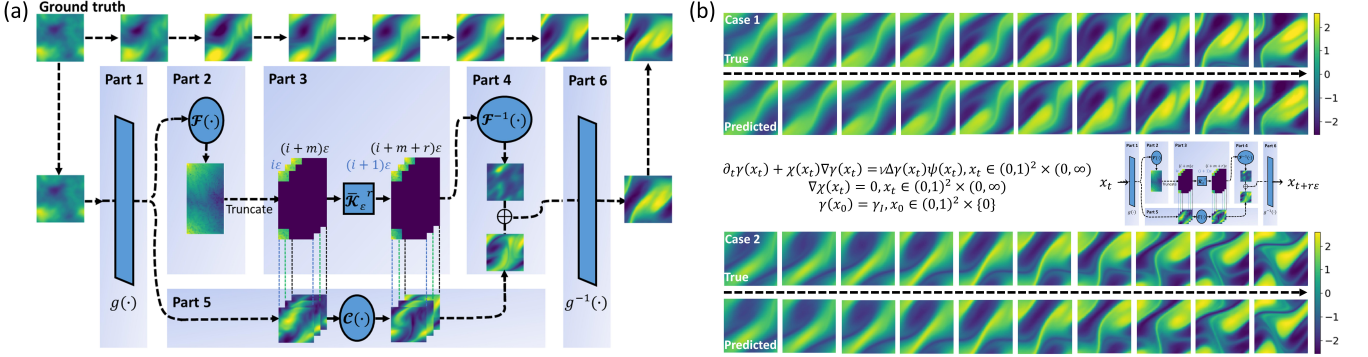


FIG. 1. Visualization of the neural network architecture of KNO and the instances of its prediction. (a) A KNO architecture is illustrated, where $r = \frac{t'-t}{\varepsilon}$ is prediction length. Note that the layout of every part is slightly reorganized to offer a clear version. (b) Two cases of the prediction results on the 2-dimensional Navier-Stokes equation with a viscosity coefficient $\nu = 10^{-4}$ are visualized, where KNO realizes a 10-second forward prediction of the equation solution given initial values. High consistency can be observed between predicted results and ground turthes.

Hankel matrix $\hat{\mathcal{H}}_{m \times n}$ to sample the Krylov sequence of $\mathbf{g}_F(\hat{\gamma}_t)$ in our computational framework (note that n equals the number of accessible samples and m is a dimension of delay-embedding). Then, we train a $o \times o$ linear layer to learn a potential Koopman operator $\bar{\mathcal{K}}_\varepsilon : \mathcal{G}(\mathbb{R}^{d_\gamma} \times T) \rightarrow \mathbb{K}$ to predict the future state as $\mathbf{g}_F(\hat{\gamma}_{t+r\varepsilon}) = \bar{\mathcal{K}}_\varepsilon^r \mathbf{g}_F(\hat{\gamma}_t)$.

- (4) *Part 4: Inverse Fourier transform.* Given each predicted state $\mathbf{g}_F(\hat{\gamma}_{t+r\varepsilon})$ in *Part 3*, we transform it from the Fourier space to $\mathcal{G}(\mathbb{R}^{d_\gamma} \times T)$ by an inverse Fourier transform, i.e., $\mathbf{g}(\hat{\gamma}_{t+r\varepsilon}) = \mathcal{F}^{-1} \circ \mathbf{g}_F(\hat{\gamma}_{t+r\varepsilon})$.
- (5) *Part 5: High-frequency information complement.* Parallel to *Parts 2-4*, we do not omit high-frequency information given its non-linear effects on $\hat{\gamma}$. Because convolutional layers can amplify high-frequency components [24], we train a convolutional layer \mathcal{C} on the outputs of *Part 1* to realize a prediction of high-frequency information, i.e., $[\mathbf{g}_C(\hat{\gamma}_{t+(r-m)\varepsilon}), \dots, \mathbf{g}_C(\hat{\gamma}_{t+r\varepsilon})]^\top = \mathcal{C}[\mathbf{g}(\hat{\gamma}_{t-m\varepsilon}), \dots, \mathbf{g}(\hat{\gamma}_t)]^\top$, where \top is transpose.
- (6) *Part 6: Inverse observation.* Given two future states, $\mathbf{g}(\hat{\gamma}_{t+r\varepsilon})$ and $\mathbf{g}_C(\hat{\gamma}_{t+r\varepsilon})$, predicted by *Parts 2-4* and *Part 5*, we unify them by $\mathbf{g}_U(\hat{\gamma}_{t+r\varepsilon}) = \mathbf{g}(\hat{\gamma}_{t+r\varepsilon}) + \mathbf{g}_C(\hat{\gamma}_{t+r\varepsilon})$. We train a non-linear decoder to represent the inverse of observation function $\mathbf{g}^{-1}(\cdot) \simeq \mathbf{g}_U^{-1}(\cdot)$ and transform $\mathbf{g}_U(\hat{\gamma}_{t+r\varepsilon})$ to $\hat{\gamma}_{t+r\varepsilon}$, the target state of equation solution.

In Fig. 1(a), we illustrate the one-unit architecture of KNO. Similar to Fourier neural operator [6], a x -unit KNO architecture can be produced by cascading the copy of *Parts 2-5* x times. The full details of KNO architecture can be seen in Sec. IV of supplementary materials (SM).

Data sets. We implement our experiments on the 1-dimensional Bateman–Burgers equation [25] and the 2-

dimensional Navier-Stokes equation [26]. Please see Sec. V of supplementary materials (SM) for data description.

Experiment designs. We conduct five experiments to validate our model: mesh-independent experiment, long-term prediction experiment, zero-shot experiment on discretization granularity, zero-shot experiment on prediction length, and ablation experiment. See Sec. IV of supplementary materials (SM) for full descriptions.

Details of implemented models. Besides KNO, we implement Fourier neural operator (FNO) [6], U-shaped neural operator (UNO) [27], convolutional LSTM (ConvLSTM) [28], and U-Net [29] for comparison. See Sec. VI of supplementary materials (SM) for details.

Mesh-independent experiment. We implement experiment on the data of 1-dimensional Bateman–Burgers equation generated under different resolutions, where FNO serves as a baseline. We implement multiple versions of KNO and FNO with different hyper-parameters (e.g., operator size o , frequency mode number f , the iteration number of the Koopman operator $r = \frac{t'-t}{\varepsilon}$ in KNO, and the width w of FNO). As illustrated in Fig. 2(a), KNO achieves almost constant prediction error on every resolution. Compared with FNO models, the prediction error of KNO models maintains more stable across different conditions. Notably, a one-unit KNO only requires about 5×10^3 parameters to outperform a one-unit FNO with more than 2×10^7 parameters, suggesting the potential of KNO to break the trade-off of accuracy and efficiency (i.e., KNO achieves higher accuracy with fewer parameters). See Sec. VI of supplementary materials (SM) for experiment details.

Long-term prediction experiment. Our long-term prediction experiment is implemented on the 2-dimensional Navier-Stokes equation, where we consider the low viscosity cases, i.e., $\nu \in \{10^{-3}, 10^{-4}\}$. In the cases where $\nu = 10^{-3}$ and $\nu = 10^{-4}$, we consider a 40-time-interval and a 10-time-interval prediction tasks, respectively. Ta-

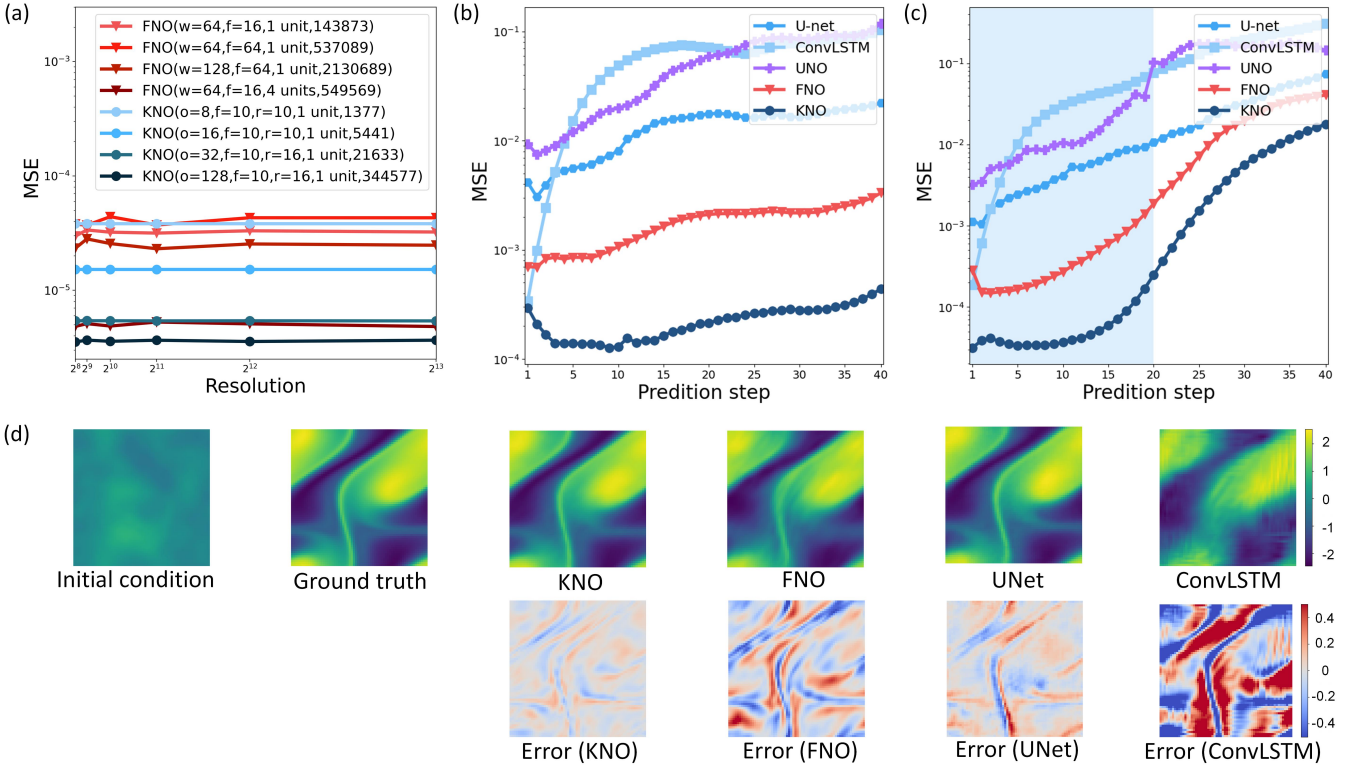


FIG. 2. Experiment results of KNO. (a) Results of the mesh-independent experiment. (b) Results of the long-term prediction experiment on the 2-dimensional Navier-Stokes equation with $\nu = 10^{-3}$. (c) Zero-shot prediction experiment concerning prediction length. (d) Visualization of prediction results on the 2-dimensional Navier-Stokes equation with $\nu = 10^{-4}$.

Models	Parameter number	Accuracy at $\nu = 10^{-3}$	Accuracy at $\nu = 10^{-4}$
FNO (default settings, one-unit)	233897	1.78×10^{-3}	2.61×10^{-2}
FNO (default settings, two-unit)	464717	2.12×10^{-4}	<u>7.72×10^{-3}</u>
ConvLSTM (default settings)	10001	6.05×10^{-2}	1.69×10^{-1}
U-Net (default settings)	24950491	1.77×10^{-3}	7.90×10^{-2}
KNO ($o = 24, f = 10, r = 12$, one-unit)	80850	3.00×10^{-4}	9.60×10^{-3}
KNO ($o = 32, f = 10, r = 12$, one-unit)	206538	2.37×10^{-4}	6.66×10^{-3}

TABLE I. Full results of long-term prediction experiment. Accuracy is measured by MSE. The best model is marked in bold while the second best one is marked by the underline.

ble 1 reports our full results, Fig. 2(b) visualizes the performance of experiment with $\nu = 10^{-3}$, and Fig. 2(d) visualizes instances of predicted results with $\nu = 10^{-4}$. These results suggest that KNO is optimal in characterizing the long-term evolution of equation solution. See Sec. VI of supplementary materials (SM) for more details.

Zero-shot experiment on discretization granularity. As suggested by Ref. [6], a mesh-independent neural operator model can be trained only on the data with lower resolution to predict the data with higher resolution (referred to as zero-shot super-resolution [6]). In our research, we validate this property by implementing a zero-shot experiment. Same as our long-term prediction experiment, there are two data sets of the 2-dimensional Navier-Stokes equation distinguished according to the viscosity $\nu \in \{10^{-3}, 10^{-4}\}$ and one data set of the 1-

dimensional Bateman–Burgers equation. The settings and objective of prediction tasks on each data set is exactly same as the long-term prediction experiment except that all models are trained on a lower resolution and tested on a higher resolution. Tables 2–3 suggest the optimality of KNO in this task. See Sec. VI of supplementary materials (SM) for experiment settings.

Zero-shot prediction experiment concerning prediction length. Because KNO is proposed to model the intricate dynamics of PDE solutions, it is natural to wonder if KNO can achieve optimal performance in zero-shot prediction with an untrained prediction length, i.e., train the model on a prediction length $t' - t = r\varepsilon$ and test it on a larger prediction length $r'\varepsilon > r\varepsilon$. This objective can be simply realized by increasing $r = \frac{t'-t}{\varepsilon}$, the iteration number of the Koopman operator, during prediction. To

Grid number	2^8	2^9	2^{10}	2^{11}	2^{12}	2^{13}
Setting 1	3.820924×10^{-5}	3.820929×10^{-5}	3.820926×10^{-5}	3.820927×10^{-5}	3.820931×10^{-5}	3.820932×10^{-5}
Setting 2	1.521201×10^{-5}	1.521201×10^{-5}	1.521200×10^{-5}	1.521202×10^{-5}	1.521202×10^{-5}	1.521200×10^{-5}
Setting 3	5.403627×10^{-6}	5.403630×10^{-6}	5.403628×10^{-6}	5.403630×10^{-6}	5.403632×10^{-6}	5.403615×10^{-6}
Setting 4	3.553927×10^{-6}	3.553980×10^{-6}	3.553943×10^{-6}	3.553957×10^{-6}	3.553942×10^{-6}	3.553938×10^{-6}

TABLE II. Zero-shot experiment (discretization granularity) on the 1-dimensional Bateman–Burgers equation. KNO settings $(o, f, r) \in \{(8, 10, 10), (16, 10, 10), (32, 10, 16), (128, 10, 16)\}$ are referred to as Settings 1-4. Accuracy is measured by MSE.

	$\nu = 10^{-3}$		$\nu = 10^{-4}$	
	32 grids	64 grids	32 grids	64 grids
FNO (default settings, one-unit)	1.78×10^{-3}	1.79×10^{-3}	1.41×10^{-2}	1.54×10^{-2}
KNO ($o = 24, f = 10, r = 12$, one-unit)	3.22×10^{-4}	3.31×10^{-4}	9.63×10^{-3}	9.60×10^{-3}

TABLE III. Zero-shot experiment (discretization granularity) on the 2-dimensional Navier–Stokes equation. Accuracy is measured by MSE.

validate the optimality of KNO in such a task, we implement an experiment on the 2-dimensional Navier–Stokes equation with a viscosity coefficient $\nu = 10^{-3}$ and 2^{12} grids. All models are trained on a time interval of $[0, 10)$ to predict the interval of $(10, 30]$ (supervised learning). Apart from the trained supervised learning task, models are also required to predict interval of $(30, 50]$, an untrained time interval. As illustrated by Fig. 2(c), KNO outperforms other models in both supervised prediction and zero-shot prediction tasks. See Sec. VI of supplementary materials (SM) for more information.

Ablation experiment. As shown in Sec. VI of supplementary materials (SM), excluding or modifying the strict combination of the observation function, the Koopman operator, and the inverse of observation function from our model (e.g., let the whole model directly implement forward prediction) reduces the accuracy significantly. Therefore, the proposed architecture design of KNO is not redundant.

Conclusion. In summary, we develop the Koopman neural operator (KNO), a mesh-independent neural-network-based solver of partial differential equations. The basic code of KNO is provided in Sec. IV of supplementary materials (SM) and the official toolbox can be seen in Ref. [30]. Compared with the existing state-of-the-art approaches, such as the Fourier neural operator, KNO exhibits a higher capacity to capture the long-term evolution of equation solution and maintain accuracy across different mesh resolutions. This property suggests the potential of KNO to be considered as a basic unit for constructing large-scale frameworks of solving complex physics equations with non-linear dynamics. Moreover, the robust mesh-independence enables KNO to be trained on the low resolution data before being applied on the high resolution data. This property may create more possibilities to reduce the computational cost of partial differential equation solving.

Acknowledgements. This project is supported by the Artificial and General Intelligence Research Program of Guo Qiang Research Institute at Tsinghua University

(2020GQQG1017) as well as the Tsinghua University Initiative Scientific Research Program.

* Correspondence should be addressed to X.R.D., P.S., and Y.T.

† Department of Earth System Science, Tsinghua University, Beijing, 100084, China.

‡ Huawei Technologies Co. Ltd., China.

§ drx17@mails.tsinghua.edu.cn; Department of Biomedical Engineering, Tsinghua University, Beijing, 100084, China.

¶ peisun@tsinghua.edu.cn; Department of Psychology & Tsinghua Laboratory of Brain and Intelligence, Tsinghua University, Beijing, 100084, China.

** tiany20@mails.tsinghua.edu.cn; Department of Psychology & Tsinghua Laboratory of Brain and Intelligence, Tsinghua University, Beijing, 100084, China.; Also at Huawei Technologies Co. Ltd., China.

[1] L. Debnath and L. Debnath, *Nonlinear partial differential equations for scientists and engineers* (Springer, 2005).

[2] M. S. Gockenbach, *Partial differential equations: analytical and numerical methods*, Vol. 122 (Siam, 2005).

[3] H. Tanabe, *Functional analytic methods for partial differential equations* (CRC Press, 2017).

[4] R. M. Mattheij, S. W. Rienstra, and J. T. T. Boonkamp, *Partial differential equations: modeling, analysis, computation* (SIAM, 2005).

[5] Z. Li, N. Kovachki, K. Azizzadenesheli, B. Liu, K. Bhattacharya, A. Stuart, and A. Anandkumar, Neural operator: Graph kernel network for partial differential equations, arXiv preprint arXiv:2003.03485 (2020).

[6] Z. Li, N. Kovachki, K. Azizzadenesheli, B. Liu, K. Bhattacharya, A. Stuart, and A. Anandkumar, Fourier neural operator for parametric partial differential equations, arXiv preprint arXiv:2010.08895 (2020).

[7] N. Kovachki, S. Lanthaler, and S. Mishra, On universal approximation and error bounds for fourier neural operators, *Journal of Machine Learning Research* **22**, Art (2021).

[8] Z. Li, D. Z. Huang, B. Liu, and A. Anandkumar, Fourier neural operator with learned deformations for pdes on general geometries, arXiv preprint arXiv:2207.05209

(2022).

[9] J. Guibas, M. Mardani, Z. Li, A. Tao, A. Anandkumar, and B. Catanzaro, Efficient token mixing for transformers via adaptive fourier neural operators, in *International Conference on Learning Representations* (2021).

[10] S. L. Brunton, M. Budisic, E. Kaiser, and J. N. Kutz, Modern koopman theory for dynamical systems, *SIAM Review* **64**, 229 (2022).

[11] A. Lasota and M. C. Mackey, *Probabilistic properties of deterministic systems* (Cambridge university press, 1985).

[12] P. Gaspard, G. Nicolis, A. Provata, and S. Tasaki, Spectral signature of the pitchfork bifurcation: Liouville equation approach, *Physical Review E* **51**, 74 (1995).

[13] P. Gaspard, Chaos, scattering and statistical mechanics, *Chaos* (2005).

[14] A. Lasota and M. C. Mackey, *Chaos, fractals, and noise: stochastic aspects of dynamics*, Vol. 97 (Springer Science & Business Media, 1998).

[15] N. Takeishi, Y. Kawahara, and T. Yairi, Learning koopman invariant subspaces for dynamic mode decomposition, *Advances in Neural Information Processing Systems* **30** (2017).

[16] O. Azencot, N. B. Erichson, V. Lin, and M. Mahoney, Forecasting sequential data using consistent koopman autoencoders, in *International Conference on Machine Learning* (PMLR, 2020) pp. 475–485.

[17] S. E. Otto and C. W. Rowley, Linearly recurrent autoencoder networks for learning dynamics, *SIAM Journal on Applied Dynamical Systems* **18**, 558 (2019).

[18] D. J. Alford-Lago, C. W. Curtis, A. T. Ihler, and O. Isan, Deep learning enhanced dynamic mode decomposition, *Chaos: An Interdisciplinary Journal of Nonlinear Science* **32**, 033116 (2022).

[19] B. Lusch, J. N. Kutz, and S. L. Brunton, Deep learning for universal linear embeddings of nonlinear dynamics, *Nature communications* **9**, 1 (2018).

[20] S. Macesic, N. Crnjaric-Zic, and I. Mezic, Koopman operator family spectrum for nonautonomous systems, *SIAM Journal on Applied Dynamical Systems* **17**, 2478 (2018).

[21] Y. Saad, *Numerical methods for large eigenvalue problems: revised edition* (SIAM, 2011).

[22] H. Arbabi and I. Mezic, Ergodic theory, dynamic mode decomposition, and computation of spectral properties of the koopman operator, *SIAM Journal on Applied Dynamical Systems* **16**, 2096 (2017).

[23] I. P. Cornfeld, S. V. Fomin, and Y. G. Sinai, *Ergodic theory*, Vol. 245 (Springer Science & Business Media, 2012).

[24] N. Park and S. Kim, How do vision transformers work?, arXiv preprint arXiv:2202.06709 (2022).

[25] E. R. Benton and G. W. Platzman, A table of solutions of the one-dimensional burgers equation, *Quarterly of Applied Mathematics* **30**, 195 (1972).

[26] C. Wang, Exact solutions of the steady-state navier-stokes equations, *Annual Review of Fluid Mechanics* **23**, 159 (1991).

[27] M. A. Rahman, Z. E. Ross, and K. Azizzadenesheli, U-no: U-shaped neural operators, arXiv preprint arXiv:2204.11127 (2022).

[28] R. Wang, K. Kashinath, M. Mustafa, A. Albert, and R. Yu, Towards physics-informed deep learning for turbulent flow prediction, in *Proceedings of the 26th ACM SIGKDD International Conference on Knowledge Discovery & Data Mining* (2020) pp. 1457–1466.

[29] O. Ronneberger, P. Fischer, and T. Brox, U-net: Convolutional networks for biomedical image segmentation, in *International Conference on Medical image computing and computer-assisted intervention* (Springer, 2015) pp. 234–241.

[30] W. Xiong, M. Ma, P. Sun, and Y. Tian, Koopmanlab: A module of koopman neural operator family for solving partial differential equations, <https://github.com/Koopman-Laboratory/KoopmanLab> (2023).